Upper Mantle Electrical Conductivity in the Himalayan Region

Baldev R. Arora[1], Wallace H. Campbell[2], and Edward R. Schiffmacher[3]

[1]*Indian Institute of Geomagnetism, Colaba, Bombay 400 005, India*
[2]*U.S. Geological Survey, Denver, Colorado, U.S.A.*
[3]*Boulder, Colorado, U.S.A.*

The electrical conductivity profile of the Earth at depths of about 50 to 500 km was determined using the quiet ionospheric current variations observed at a line of stations near 75° East longitude. We found conductivity values of about 0.06 S/m from 50 to approximately 350 km depth with slight relative maxima near 125 and 275 km, interspersed by relative minima near 210 and 330 km. Thereafter, the conductivity increased sharply toward a value of about 0.18 S/m at 500 km with no indication of leveling off. A comparison with regional seismic wave-velocity models shows good correspondence between high conductivity and low-velocity zones. The conduction by hydrogen-saturated pyroxene is envisaged as a possible mechanism for the high conductivity and its variation in the upper mantle.

1. Introduction

When an oscillating current source flows above a conducting half-space a current is induced to flow in the conductor. The depth to which the induced current flows in dependent upon the source wavelengths and the conductivity-depth profile. The field measured at the surface of the conducting medium is a complex mixture of the source and induced parts. When these parts can be mathematically separated into their external (source) and internal (induced) polynomial representations, the phase and amplitude relationships can be used to determine conductivity within the induction medium. Because of the almost radial symmetry of the conducting region of the Earth's mantle and the well-behaved ionospheric current on days of the quiet geomagnetic field, special mathematical techniques can be used to determine the equivalent conductivity-depth profile of the Earth that could produce the observed surface field patterns.

The probing source field for our study is the ionospheric dynamo current system obtained from the geomagnetically quiet days of 1976 and 1977, at 18 observatories established near 75°E longitude extending from the geomagnetic equator to the polar region (Campbell *et al.*, 1992, 1993). Of the original 18 observatories, whose data were sued for the characterization of *Sq* source currents, the distribution of 13 stations, scanning the region of *Sq* vortex (0° to 60°N), is shown in Fig. 1. The data from one of the high latitude station NYDA (Geograph. 66.6°N, 73.0°E), not marked in Fig. 1, was rejected for failing to meet self-consistency tests. Another station, marked on figures as SHL, was eliminated on the grounds of its long offset from 75° longitude line chosen as the principal longitude. The large number, close alignment and full two-year operation of the observatories made them particularly suitable for the present study. Spherical harmonic analysis (SHA) technique used to separate the external and internal fields was that presented by Campbell (1990) for a longitudinal chain of observatories in one hemisphere. The present authors described the application of that method to the 75°E chain in Campbell *et al.* (1993). We will now use the SHA coefficients derived from that study to determine the deep-Earth conductivity.

Schmucker (1970) devised the method of determining the equivalent electrical conductivity profile from the SHA external and internal field coefficients. Schmucker's method has been shown to be equivalent to other conductivity profile transformations (Weidelt *et al.*, 1980; Jones, 1983; Schmucker, 1987). Campbell and Anderssen (1983) and Campbell (1989) elaborated on this technique for application
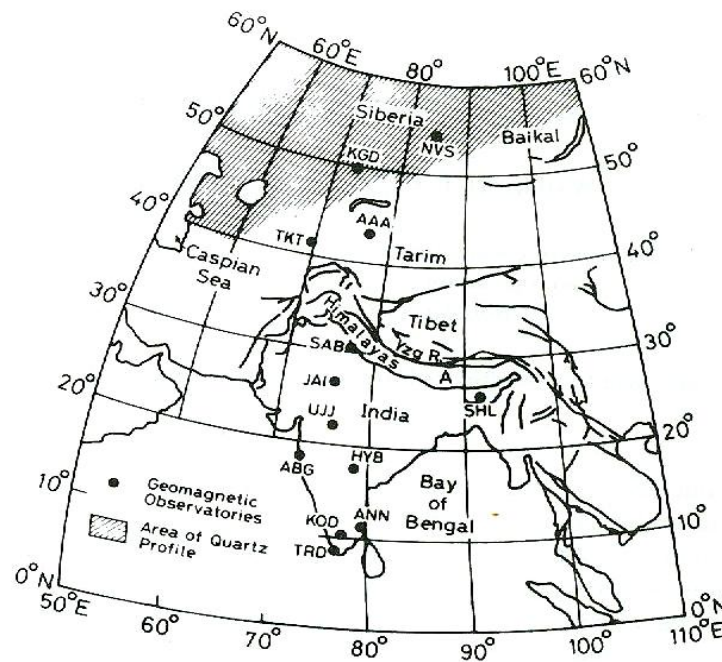
Fig. 1. Distribution of geomagnetic observatories along the India-Siberia region used in the present study. IAGA codes for the observatories are also indicated alongside the observatory location. The hatched area marks the region of northern Eurasia covered by the Deep Seismic Sounding Quartz profile, used in estimating the upper mantle velocity structure shown in Figs. 4(a) and (b).

to the continental Sq systems. Campbell and Schiffmacher (1988), compared the seven continental region upper mantle conductivities using the International Quiet Year 1965 geomagnetic data set.

2. Analysis Method

Let us introduce the description of the analysis with an overview that emphasizes some of important features that make possible this conductivity profile determination. More complete details are provided in the above references. The method of analysis starts with the differential equations Maxwell (1873) derived to compress into a coherent form the electromagnetic laws (Faraday, Biot-Ssvart, etc.) found in laboratory experiments. The magnetic fields represented by these equations are from either "real" currents to currents that could be considered "equivalent" or "substitute". That is, the fields from such current flow would be indistinguishable from that of the realistic current flow.

For the conditions of measurements of field about the surface of a sphere across which current does not flow, Maxwell's differential equations were given a separable, series solution by Gauss (1838) for his spherical harmonic analysis (SHA) of the Earth's main field. The "separable" features means that separate solutions for each of the three direction variables were obtained. The separated radial solution allowed a division into parts that must be external and parts that must be internal to the surface of measurement location. In Gauss's series solution, each term of the solution can represent a field component, independently abiding the electromagnetic laws that the Maxwell equations represent. For the external and internal parts separately, these are individual spherical harmonic polynomial (Legendre) terms, each having two indices, m and n, representing the field as a series of currents that satisfy the physical laws.

Schuster (1889, 1908) applied the Gauss SHA technique to the quiet daily field variation (Sq) to prove that the source was currents external to the Earth's surface. Chapman (1919, also see Chapman and Bartels, 1940) made the first significant Earth conductivity determinations with the separated external and internal fields. He popularized the technique of considering the magnetic observatories moving under an external equivalent Sq current system fixed with respect to the Sun so that the 24-hour Sq variation at a

station represented 360° of Longitudinal track about the Earth. Matsushita and Maeda (1965) made the next major contribution by separating out North-South Hemisphere sectors for determining the sectorial external and internal Sq fields.

Schmucker's (1970) contribution was to provide equations for describing a conductivity and depth where could flow an equivalent induced internal current for the SHA fields. Small flaws in Schmucker's paper were corrected by Campbell (op. cit.) who introduced three innovations to the conductivity profiling with the quiet field variations: 1) Continental half-sectors were isolated for analysis by a special mathematical technique that cloned a sphere (necessary for the Gauss separation) from the area of interest; 2) Equations representative of the equivalent Sq currents for each day of the seasonal variation in the analysis period were established so that sets of external and internal fields could be computed for a great many days; 3) Then the many (for each separated polynomial and each day) conductivity-depth determinations (where equivalent currents could flow) provided a scatter of values to which Cleveland's (1979) method was employed to find a unique, locally weighted, continuous regression curve for the sought profile (and corresponding measures of fit robustness).

Inherent to the determinations, starting with Maxwell's equations, is the fact that only "equivalent (substitute)" currents can be determined. It must be left to other information, such as geologic sampling, seismic-level correspondences, and laboratory high temperature/pressure tests, to determine the reality of the conductivity profiles.

We now summarize the important formulae from Campbell (1989), used in the conductivity determination. Calling $(a_{ex})_n{}^m$ and $(b_{ex})_n{}^m$ the external cosine and sine, spherical harmonic, Gauss coefficients (and similarly for the internal $(a_{in})_n{}^m$ and $(b_{in})_n{}^m$, where n and m are the SHA degree and order, we call the coefficient sums

$$A_n^m = \left(a_{ex}\right)_n^m + \left(a_{in}\right)_n^m \quad \text{and} \quad B_n^m = \left(b_{ex}\right)_n^m + \left(b_{in}\right)_n^m. \tag{1}$$

Then the depth to a conducting layer that can produce the observed fields is given by

$$d_n^m = z - p \text{ kilometers} \tag{2}$$

for a conductivity of

$$\sigma_n^m = \frac{5.4x10^4}{m\left(\pi p\right)^2} \text{ Siemens / meter} \tag{3}$$

where, with R as the Earth's radius in kilometers,

$$z = \frac{R\left\{A_n^m\left[n\left(a_{ex}\right)_n^m - (n+1)\left(a_{in}\right)_n^m\right] + B_n^m\left[n\left(b_{ex}\right)_n^m - (n+1)\left(b_{in}\right)_n^m\right]\right\}}{n(n+1)\left[\left(A_n^m\right)^2 + \left(B_n^m\right)^2\right]} \tag{4}$$

and

$$p = \frac{R\left\{A_n^m\left[n\left(b_{ex}\right)_n^m - (n+1)\left(b_{in}\right)_n^m\right] - B_n^m\left[n\left(a_{ex}\right)_n^m - (n+1)\left(a_{in}\right)_n^m\right]\right\}}{n(n+1)\left[\left(A_n^m\right)^2 + \left(B_n^m\right)^2\right]} \tag{5}$$

form the real and imaginary parts of the transfer function

$$C_n^m = z - ip. \tag{6}$$

The ratio of the internal to external components of the surface field is given by

$$S_n^m = u + iv \tag{7}$$

where

$$u = \frac{\left(a_{\text{ex}}\right)_n^m \left(a_{\text{in}}\right)_n^m + \left(b_{\text{ex}}\right)_n^m \left(b_{\text{in}}\right)_n^m}{\left[\left(a_{\text{ex}}\right)_n^m\right]^2 + \left[\left(b_{\text{ex}}\right)_n^m\right]^2} \tag{8}$$

and

$$v = \frac{\left(b_{\text{ex}}\right)_n^m \left(a_{\text{in}}\right)_n^m - \left(a_{\text{ex}}\right)_n^m \left(b_{\text{in}}\right)_n^m}{\left[\left(a_{\text{ex}}\right)_n^m\right]^2 + \left[\left(b_{\text{ex}}\right)_n^m\right]^2}. \tag{9}$$

There are three limitations on the values for the analysis. The SHA coefficient amplitudes must not be too small:

$$\left[\left(A_n^m\right)^2 + \left(B_n^m\right)^2\right]^{0.5} \geq G_n^m \text{ nT.} \tag{10}$$

For earlier conductivity determinations (e.g. Campbell and Anderssen, 1983; Campbell and Schiffmacher, 1988) the cutoff values of G_n^m were tailored to decrease with increasing m in proportion to the decreasing amplitudes of the Sq field harmonics defined by the (24/m)-hr components. When extensive tests were made on the present data set either making the above m adjustments to G_n^m or by simply assigning it a constant value for all m's, no significant difference was seen. The effect of changing cut off values of G_n^m upon the conductivity-depth profile is investigated in later section.

Also, it is required that

$$0 \geq \arg\left(C_n^m\right) \geq -45 \tag{11}$$

and

$$80 \geq \arg\left(S_n^m\right) \geq 10. \tag{12}$$

There are two interesting features involved in the application of this conductivity determination method to the Sq current sources. These features are related to the fact that the effective wavelengths for the SHA representation of the field along a longitude line equals $(n - m + 1)$. First, the polynomial terms having values of $(n - m) > 1$ have been shown to arise primarily from the currents flowing at polar latitudes, due to low-level solar terrestrial disturbances, not from the usual quiet-time ionospheric dynamo currents

(Campbell, 1990; Campbell *et al.*, 1993). Thus, our analysis will avoid these higher Legendre wavelengths as contributions outside our region of interest. Second, the principal contribution to the potential function defining *Sq* comes from fields that describe the region of the major *Sq* current vortex. Such fields are best represented by the dominant $(n - m) = 1$ polynomial terms (Campbell, 1990). The focus of this vortex varies seasonally between 22° and 29° geomagnetic latitude for the India-Siberia data set (Campbell *et al.*, 1993), scanning the region of the Himalayan Mountains. Therefore, the reduced conductivity-depth profile is specially sensitive to the Himalayan Mountains region.

Our conductivity method involves the use of a large number of determinations and the application of several statistical fitting procedures. The analysis starts with the Fourier representation of the three, orthogonal, quiet-field components at each station, determining their best-fit daily variation as well as the two-year seasonal changes. Next there is a polynomial fitting of the latitudinal variation of the station field Fourier components. These two steps are described in Campbell *et al.* (1992). Then there were 48 separate spherical harmonic determinations, fitting the *three-component* external and internal quiet fields on the 06th and 21st of each month of 1976 and 1977. The SHA procedure used spherical polynomials up to degree $n = 23$ and order $m = 6$. About 150 paired values of conductivity and depth were obtained in the typical determination with the restriction of $(n - m) = 1$. These values were then fitted to a unique profile using the locally weighted regression technique (called "Lowess") of Cleveland (1979) with a smoothing factor of 0.5 and two fitting iterations. Cleveland's method (op. cit.) also provides an index of robustness of the fit for each point, with values ranging from 0 to 1.

3. Results

In this section we will describe the equivalent electrical conductivity profile from about 50 to
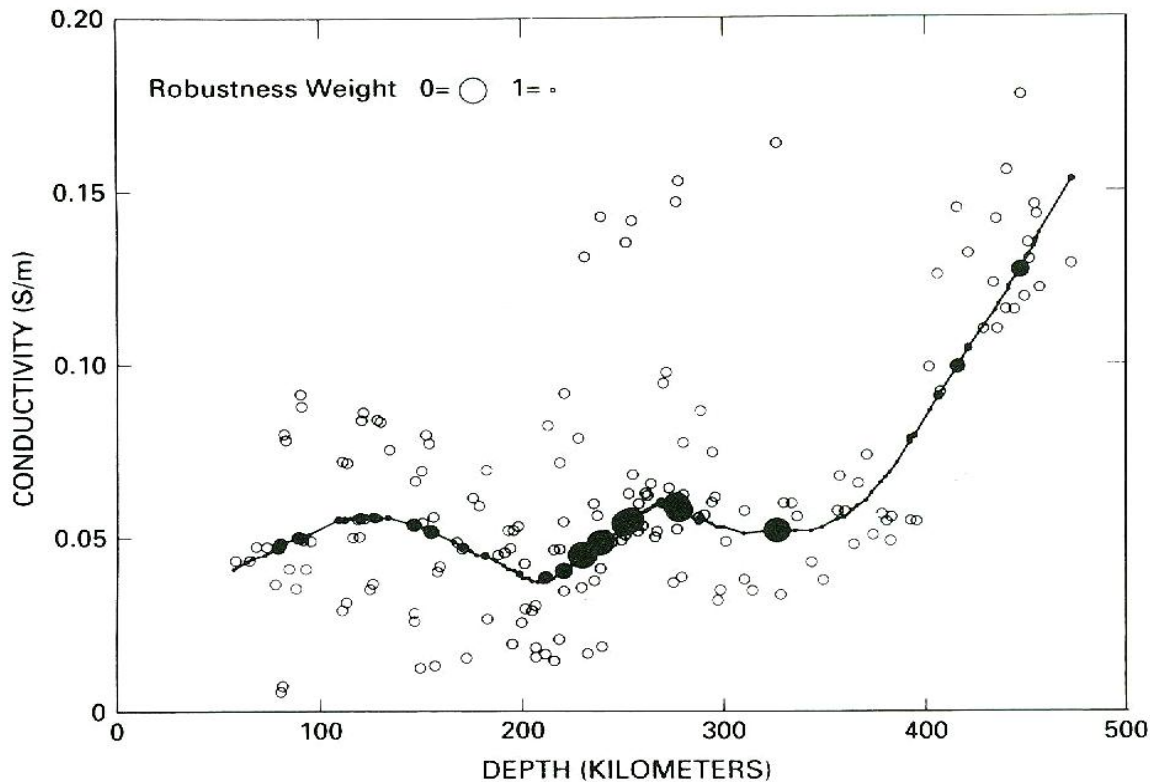

Fig. 2. Computed conductivity (Siemens/meter) versus depth (kilometers) data points (scattered values) and locally weighted fit (solid line) of these values. Robust weighting of the points for the regression fitting (Cleveland, 1979) is indicated by the solid circle sizes: 0.0 (poorest) for circles of radius similar to that near 325 km depth and 1.0 (best) for circles of radius similar to that near 50 km depth.

500 km depth using two figures. We will use the first figure to demonstrate the robust fitting of the individual values. The second figure illustrates the effect of field amplitude limitations on the profile (Eq. (10)).

The scattered, small, open circles in Fig. 2 show 152 conductivity-depth data values computed using a low amplitude cutoff value of G_n^m at 0.5 nT. The locally weighted, regression fitting of these values is given by the solid line, computed via the best fit, Lowess technique. The size of the solid circles at positions near the line indicate the robustness of the fitting. The largest circle, near 325 km depth, corresponds to approximately 0 robustness; the smallest circle, near 50 km depth, corresponds to 1.0 robustness. Note the
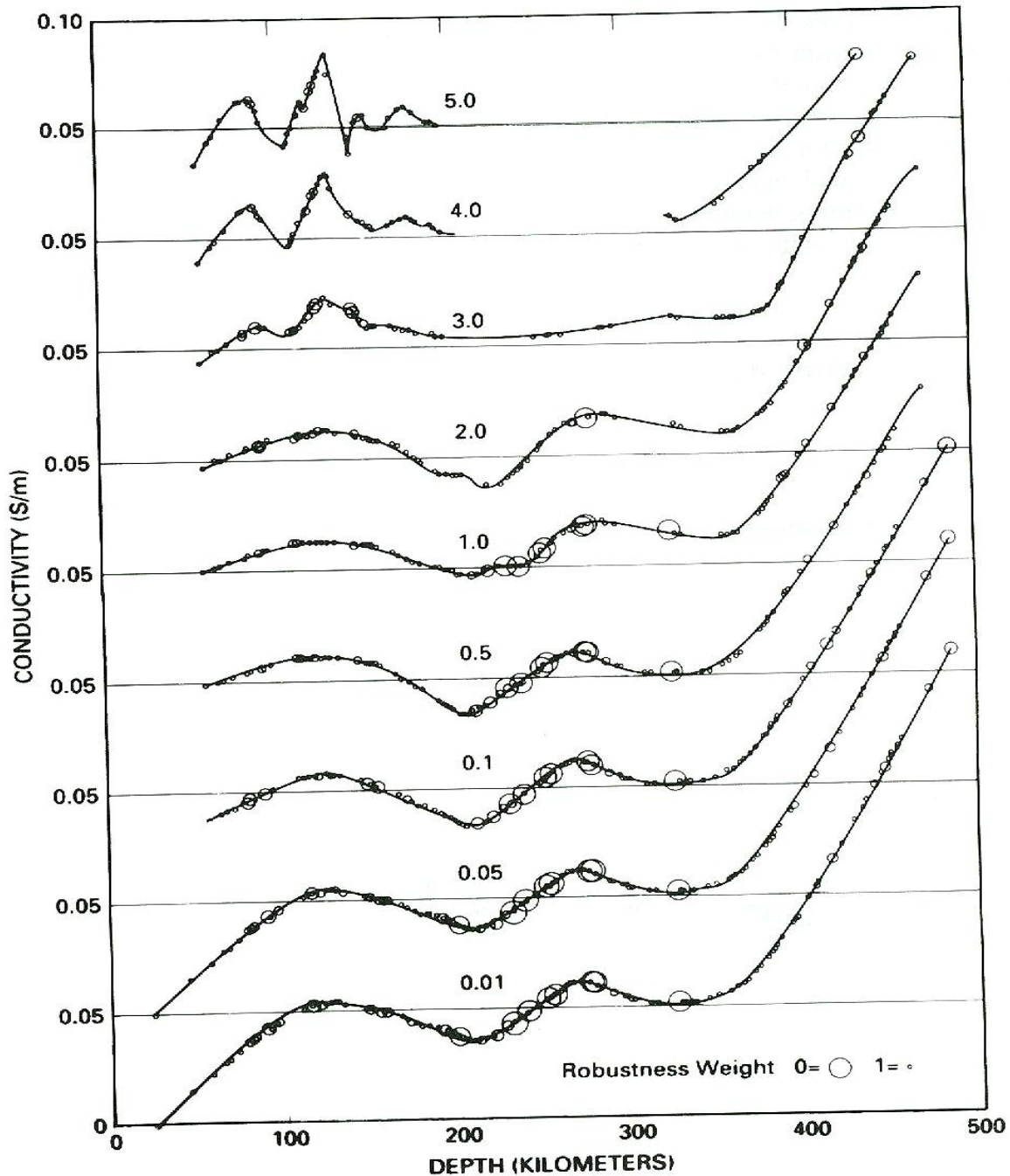

Fig. 3. Stacked-plot of conductivity-depth determinations for variation of low-amplitude cutoff value, G_n^m in nT. The number of values for the determinations varies from 187 points for the .01-nT level to 48 points for the 5.0-nT level.

region of low robustness between 200 and 300 km, where the data are not well clustered.

A scatter in conductivity-depth values occurs for several reasons: (a) the determination of the Sq fields has variations imposed from irregularities in the source region and the station field scalings have equipment and scaling irregularities so the fitting harmonics exhibit some scatter of values from day to day; (b) the Sq source current moves its average position through the year and from year to year so that the sample region, emphasized beneath the source current focus, shifts position for the different samples; and (c) latitude smoothing of the representative fields is carried out separately for the three field components as independent variables, introducing some error scatter because the SHA is simultaneously fitted to all three components that are not independent.

Despite the large scatter, the general features of conductivity variations with depth, exhibited by the Lowess fitting, can also be traced in the upper and lower envelop to the scattered values, perhaps except for a small group of seven values near 0.15 S/m (between about 200 and 300 km depth). It is not clear whether these are the outliers or whether there are times when the varying source Sq field is inducing a response from a small scale, high conductivity anomaly at that location. One such possible conductive structure, shown to produce induction effects at Sq periods, was revealed by the magnetometer array study over NW India (Arora *et al.*, 1982).

We see the conductivity rising-from low sub-crustal values to a relative maximum of about 0.06 S/m-near 125 km depth. A relative minimum of about 0.04 S/m appears near 210 km, followed by another relative maximum of about 0.07 S/m, near 275 km. After another relative minimum near 325 km the conductivity rises rapidly toward a value of 0.18 S/m at 500 km depth with no sign of leveling off.

In Fig. 3 the same external and internal SHA coefficients are used to explore the effect of changing the low amplitude cutoff value of G_n^m from 0.01 nT (represented by 187 data points) to 5.0 nT (represented by 48 data points). If the selected value is too low, the background noise level is entered; if the selected value is too high, too few conductivity determinations are obtained to define a profile. The 0.01 and 0.05 nT traces are identical, indicating that the $arg(C_n^m)$ and $arg(S_n^m)$ restrictions are limiting the sample size rather than G_n^m at this level. The Lowess data-fitting remains essentially unchanged up through the 2.0 nT level (represented by 113 data points). Note that at this level the robustness is quite high at all but one point and we therefore gain renewed confidence in the significance of the relative maximum near 275–280 km. At the 3.0 and 5.0 cutoff values the sample size had diminished to 86 and 56 points. These were seen to be insufficient numbers for effective application of a Lowess regression fitting. The disappearance of the 275 km peak at a cutoff value of 3 nT or break in the conductivity-depth profile at still higher cutoff amplitude may simply be due to relatively a few or rather no estimates in this depth range. We conclude that cutoff values between 0.1 and 2.0 nT can provide suitable and consistent conductivity profiles for the Himalayan data set. We chose to work with the cutoff level of 0.5 nT which, provided 152 data points.

4. Discussion

4.1 General features of conductivity-depth profile and their correlation with other regional models

The present work, both in respect of the nature of the data (daily field variations) and analysis techniques adopted, either to approximate source field geometry or to invert the electromagnetic response functions to conductivity-depth profile, is similar to the one employed by Campbell and Schiffmacher (1988—hereafter called Paper I). They determined the conductivity-depth profile for seven continental regions, including a Central Asia region which overlaps the present study area. However, in contrast to the seven stations along the Asian sector used in Paper I, 16 observatories evenly distributed between equator and geomagnetic pole are presently used. This permitted a better approximation of the spatial characteristics along a line of longitude, resulting in better estimation of the conductivity distribution in the depth range of 50–350 km. Storm-time (D_{st}) variations with period greater than 3 days have been used to determine conductivities well below 300 km (Schmucker, 1984; Tarits, 1992; Constable, 1993a). Magnetotelluric soundings provide information on the conductivity distribution at depths of below 200 km only in exceptional cases. The significance of Sq-field use stems from the fact that it provides the

required spatial and frequency composition to fill vital gaps in the depth range of 50–400 km. Largely because of the difficulties in approximating the complex Sq source field adequately from a limited number of observatories and the concern regarding the Sq sensitivity to surface (e.g. ocean) or shallow lateral conductivity hetrogeneities (cf. Roberts, 1986), the Sq data have often been ignored in regional induction studies. The present analysis, however, documents convincingly, that given the appropriate distribution of observatories for describing the source field through spherical harmonic expansion, the inversion of the response functions corresponding to various combinations of spherical harmonics with $n - m = 1$, yields the conductivity depth profile as an almost continuous function of depth, from 50 to 500 km (Fig. 2).

An interesting feature of the conductivity-depth profiles is that the uppermost mantle can be viewed as a stack of inhomogeneous layers, in variance with the global model obtained under the assumption of a spherically symmetric Earth (Banks, 1972; Berdichevski *et al.*, 1979; Fainberg and Rotanova, 1974; Parkinson, 1974, Hobbs, 1987). These authors used a zero-degree (symmetric) distribution model in which the upper mantle down to 400–500 km depth is seen as a single homogeneous layer (perhaps as a consequence of averaging lateral conductivity variations). In terms of the rapid rise below 350–500 km depth, the present model (Fig. 2) is similar to the global models, which show a rapid increase somewhere in the depth interval of 400–800 km (Schultz and Larsen, 1990). The sharp character of conductivity rise below 350–400 km depth, noted in paper I beneath Central Asia, persists in Fig. 2 and supports the earlier inference of Campbell and Schiffmacher (1988) that, below 400 km depth, the upper mantle beneath Central Asia and Africa shows the highest conductivities of the seven continental regions.

The conductivity variation in the 50–300 km depth range is marked by well resolved peaks centred at 125 km and 275 km, separated by a well marked minimum at 200 km. The persistence of the conductivity distribution pattern in Fig. 3, at different cutoff levels of amplitude, suggests that the statistical approach to the determination is reliable, despite the fact that individual estimates show large scatter (Fig. 2). A rise in conductivity, similar to our result was seen at depths of around 100–150 km on the European conductivity profile in Paper I. The presence of a conducting layer beneath the Fennoscandian shield in the depth interval of 100–150 km was also reported by Jones (1982). The broad agreement between the average depths of the conducting layer beneath the Central Europe, Fennoscandian shield and Central Asia sectors, the layer with enhanced conductivity at a depth of 125–150 km may be interpreted to correspond with the lithosphere-asthenosphere transition.

A moderate electrical inhomogeneity at 275 km depth, under the central Asian sector, is indicated in Fig. 2. To account for the observed electromagnetic response at Sq and D_{st} periods, Schmucker (1984) suggested a subdivision of the upper mantle into two layers underlain by a uniform conducting substratum. His first model—SCH (1)— is sufficient to explain the observed response within error limits. However, he also demonstrated that introduction of another more conducting layer between the two upper mantle layers—SCH (2)—improves the fit marginally and is also able to account for the response at shorter periods better than model SCH (1). More recently Bahr *et al.* (1993) inverting the combined MT and magnetic field variations data from western Europe, at periods between 3 hours to 600 hours, observed that a single conductivity jump at either 400, 500 or 700 km cannot explain the broadband data. The smallest misfit was obtained from a model including an intermediate conductive layer at 300–400 km depth and a large conductivity increase at 670 km depth. The location of the intermediate conducting layer, both in the models of Schiffmacher (1984) and Bahr *et al.* (1993), is in fair agreement with the moderately conducting layer indicated in Fig. 2.

The conversion of smooth global models of mantle electrical conductivity distribution, using a laboratory based conductivity-temperature (σ-T) relationship for dry, subsolidus olivine, yields a temperature of 1750°C at a depth of 410 km (Duba, 1976; Constable, 1993a). This temperature is much higher than an independent estimate of 1400°C at 410 km based on laboratory values of the temperature-pressure for the $\alpha \rightarrow \alpha + \beta$ transition in olivine (Katsura and Ito, 1989). Constable (1993a), has shown that allowing a sharp boundary in conductivity at the 670-km seismic discontinuity in the regularized conductivity inversion of global geomagnetic response functions, lowers the electrogeotherm to about only 1600°C at 410 km. He, however, showed that the currently predicted value of 1400°C at the $\alpha \rightarrow \alpha + \beta$ transition

can be achieved by incorporating a more conducting layer above 200 km. The present evidence on the presence of additional layers of marginally enhanced conductivity above the 410-km discontinuity may lend support to the hypothesis of Constable (1993a).

4.2 Correlation with seismic wave-velocity structure

The current seismic wave-velocity models for the mantle, such as PREM (Dziewonski and Anderson, 1981) and IASP 91 (Kennett and Engdahl, 1991) show an abrupt rise in velocity at 410 km and 670 km depth and provide strong evidence for the existence of a zone of low velocity gradient between about 100 and 220 km depth. The controlled-source, high-resolution, deep, seismic soundings along long distance profiles have begun to provide new insight on the upper mantle velocity distribution on a regional scale. More recently, Mechie et al. (1993) have modelled the mantle velocity structure beneath northern Eurasia using peaceful nuclear explosions. Their models are reproduced in Figs. 4(a) and (b). Incorporating a large part of the region defined by the northern half of the observatory line used in the present analysis, they reveal that down to 200–250 km depth in the upper mantle, essentially two major zones or layers, separated by a 30–40 km thick transition zone, can be identified. The upper of these zones, through which Pn waves propagate, extends down to about 100 km and is ascribed a velocity of 8.1 to 8.3 km/sec. The second layer, starting from 130–140 km depth, extends down to 200–250 km and consists of alternating high and low velocity layers (8.4–8.7 km/sec). This laminated, uppermost mantle was found to overlie a low velocity (8.3–8.5 km/sec) zone from about 200 to 300 km depth. The transition zone between 100–140 km depth range and a low velocity zone stretching between 200–300 km, both in respect of the thickness and central location, show a very good correspondence with the high conductivity zones indicated by the present study (Fig. 4(d)). An alternative velocity-depth model by Beghoul et al. (1993), for the Tibetan Plateau (Fig. 4(c)) indicates the unmistakable presence of a low-velocity zone centred around 275 km, which is in excellent agreement with the present results. The absence of any velocity discontinuity in the uppermost mantle in this model is an artifact of the modelling, wherein the upper mantle from the base of the crust to a depth of 220 km is treated as a single entity. However, it is worthy of note that surface dispersion studies of Hwang and Mitchell (1987) indicated a low velocity layer for S-waves between 100 and 110 km beneath the Himalaya. The general correspondence noted between high conductivity zones and low velocity zones here is in agreement with the global results of Tarits (1992), although the mechanism of these correlations still remains elusive.

Most of the seismic wave-velocity studies in India have focussed on the structure of the crust and have
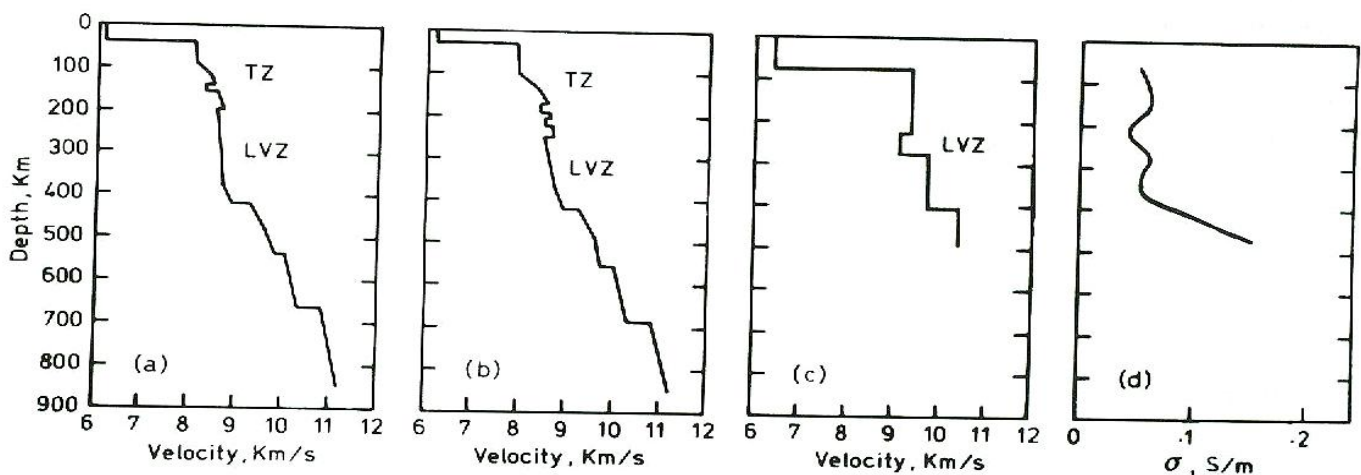

Fig. 4. P-wave velocity-depth models for northern Eurasia derived using Peaceful Nuclear Explosions as recorded on the (a) northern and (b) southern parts of the Quartz Profile (adopted from Mechie et al. (1993). (c) gives the average P-wave velocity model for Tibet (Beghoul et al., 1993). (d) The smooth best fit conductivity-depth profiles given by solid line in Fig. 2, is also included.

provided velocity information only down to the depths of 200–300 km or so. (For review see Ram and Singh, 1982; Bhattcharya, 1992). Upper mantle velocity models, extending down to depths pertinent to the present discussion, have been reported by Ram and Mereu (1977), for four seismic zones of India and contiguous regions defined by four azimuthal sectors. Clear evidence for the existence of "410-km" and "670-km" discontinuities was evident in all seismic zones except in the Himalayan region. In the latter region, the "670-km" discontinuity is replaced by a very broad velocity gradient zone and the velocity increases steadily below the depth of the "410-km" discontinuity. It is interesting to note that on the conductivity-depth profile in Fig. 2, which are sensitive to the conductivity distribution below the Himalaya, the broad, high-velocity gradient zone is characterized by a steep rise in conductivity below 400 km, reaching the highest conductivities of the seven continental regions. The noted correlation might be an indirect manifestation of a common process acting differently on both parameters.

4.3 Possible mechanisms for enhanced upper mantle electrical conductivity

The steep increase in conductivity around 400 km depth, seen in this regional and on many sub-continental profiles (Campbell and Schiffmacher, 1988; Schultz, 1990), are generally related to a phase transition of the mantle material from olivine to spinel structure (Adam, 1980; Akimoto and Fujisawa, 1965; Omura, 1991). A second β-γ phase transition has been postulated to produce discontinuous conductivity change around 520 km (Omura, 1991) whereas often reported discontinuity around 670 km is believed to result from chemical compositional change. The $\alpha \rightarrow \beta$ phase transition and chemical composition changes are also believed to cause the discontinuous increase in seismic wave-velocities at the well established 410- and 670-km discontinuities (Dziewonski and Anderson, 1981). However, the validity of the phase transition mechanism for conductivity enhancement is doubted by Duba (1992) and Duba and von der Gönna (1994) who have enumerated the difficulties of simulating these transitions in laboratory models because of no control on oxygen fugacity.

Further observational evidence that estimated, upper mantle electrical conductivity exceeds the laboratory value of conductivity for dry olivine has led many to suggest the existence of partial melt as a possible mechanism for high upper mantle conductivity (Shankland and Waff, 1977). Lately, some alternative mechanisms such as grain boundary carbon films have also been advanced (Shankland *et al.*, 1981). In more recent years, Karoto (1990) has shown, that if some hydrogen were dissolved in the olivine lattice, then the high conductivity of the upper mantle could be attributable to solid-state conduction. The recent hydrothermal experiment of Bai and Kohlstedt (1992) on olivine single crystals showed that olivine at temperature of 1300°C and 50–300 MPa can accommodate as much as 0.0034 wt% water. This observational evidence on the existence of hydrogen phase were considered to corroborate Karoto's idea that considerably greater thermal stability and mobility of hydrogen may account for the high conductivity of the asthensphere. However, Constable (1993b) has argued that high concentration of hydrogen required to enhance the upper mantle conductivity sufficiently conspires the hydrogen conduction mechanism to be less effective than postulated by Karoto (1990). The infrared spectrascopy measurements of Bell and Rossman (1992) on nominally anhydrous mantle minerals, obtained from mantle derived xenoliths, suggest presence of hydrogen in hydroxyl (OH) group. Their results indicated that, of the major mantle minerals such as olivine, pyroxenes and garnet, pyroxenes are the most hydrous, typically containing 200 to 500 parts per million (H_2O) by weight, dominating the water budget and hydrogen geochemistry of mantle rocks. Although the measurements on xenolith suites obtained from the upper 150 km of the mantle are valuable in demonstrating the availability of hydrous phases as repositories for mantle water, these observations are not easily generalised to average mantle.

Independent, experimental, phase-equilibrium studies on water-rich mantle-analogue compositions—MgO-SiO_2-H_2O, have also produced hydrous phases, but their stability at the high, average temperatures and pressures of the mantle remains to be documented (Bell, 1992). Experimental studies on mica and amphiboles reveal that some minor constituents (e.g. sodium, potassium, titanium and fluorine) tend to stablise some of the hydrous or humite group minerals phases at mantle pressures and temperatures. However, as the incompatible element content of the upper mantle is low and large concentrations of K,

Ti and F-rich hydrous minerals cannot be supported throughout the mantle, Bell hypothesized (1992) that hydrous minerals may be restricted to areas or layers enriched in these elements, with the water storage sites depending on the scale of mantle chemical heterogeneities.

The new laboratory experiment on the $MgO-SiO_2-H_2O$ volatile bearing system, under high pressure-temperature conditions, led Gasparik (1991) to suggest that solidification of multi-component, fractionated, magma ocean at the last stages of Earth accretion produced a stratified upper mantle. This solidification, which took place at an extremely high temperature, produced an olivine-rich upper layer and a garnet-rich lower layer and was completed by a crystallization of pyroxene, which is always the last phase to crystallize. It was Gasparik's opinion that this crystallization of residual melts, enriched in sodium, iron, potassium, incompatible elements and volatiles, produced a pyroxene-rich intermediate layer at 300–400 km depths, which he called "anti-crust". Because the concentration of hydrous phases in the upper mantle is linked with potasium bearing pyroxene, the "anti-crust" in the petrological model of Gasparik (1991) appears to be an important reservoir of hydrogen above the transition zone. With a view of estimating the effect of hydrogen mobility as a source of high conductivity at depths of the anti-crust, it will be important to investigate experimentally the solubility and diffusivity of the hydrogen in the anti-crust composition system, at a temperature and pressure relevant to this depth range, in a manner similar to the experiment of Bai and Kohlstedt on olivine. A better understanding of the effect of pressure and temperature on the solubility of Hydrogen in pyroxene may also help to eluciate whether a marginal enhancement of conductivity seen here, in the depth range of 250–300 km, may be a manifestation of fluctuations in depth of the anti-crust beneath the compressional collisional regime of the Himalaya.

REFERENCES

Adam, A., Relation of mantle conductivity to physical conditions in the asthenosphere, *Geophys. Surv.*, **4**, 43–55, 1980.

Akimoto, S. and H. Fujisawa, Demonstration of the electrical conductivity jump produced by the Olivine-Spinel transition, *J. Geophys. Res.*, **70**, 443–449, 1965.

Arora, B. R., F. E. M. Lilley, M. N. Sloane, B. P. Singh, B. J. Srivastava, and S. N. Prasad, Geomagnetic induction and conductive structures in north-west India, *Geophys. J. R. astr. Soc.*, **69**, 459–475, 1982.

Bahr, K., N. Olsen, and T. J. Shankland, On the combination of the magnetotelluric and the geomagnetic depth sounding method for resolving an electrical conductivity increase at 400 km depths, *Geophys. Res. Lett.*, **20**, 2937–2940, 1993.

Bai, Q. and D. L. Kohlstedt, Substantial hydrogen solubility in olivine and implications for water storage in the mantle, *Nature*, **357**, 672–674, 1992.

Banks, R. J., The overall conductivity distribution of the Earth, *J. Geomag. Geoelectr.*, **24**, 337–351, 1972.

Beghoul, N., M. Barazangi, and B. Isacks, Lithospheric structure of Tibet and western north America: Mechanisms of uplift and a comparative study, *J. Geophys. Res.*, **98**, 1997–2016, 1993.

Bell, D. R., Water in mantle minerals, *Nature*, **357**, 646–647, 1992.

Bell, D. R. and G. R. Rossman, Water in Earth's Mantle: The role of nominally anhydrous minerals, *Science*, **255**, 1391–1396, 1992.

Berdichevski, M. N., L. L. Vanyan, L. P. Lagutinskaya, N. M. Rotanov, and E. B. Fainberg, The experience of the Earth frequency sounding by the results of the spherical harmonic analysis of geomagnetic field variations, *Geomagn. Aeron.*, **10**, 374–377, 1979.

Bhattacharya, S. N., Crustal and upper mantle velocity structure of India from surface wave dispersion, *Current Science*, **62**, 94–100, 1992.

Campbell, W. H., The regular geomagnetic field variations during quiet solar conditions, Chap. 6, in *Geomagnetism*, Vol. 3, edited

by J. A. Jacobs, pp. 385–460, Academic Press, London, 1989.

Campbell, W. H., Differences in geomagnetic *Sq* field representations due to variations in spherical harmonic analysis techniques, *J. Geophys. Res.*, **95**, 20923–20936, 1990.

Campbell, W. H. and R. S. Anderssen, Conductivity of the subcontinental upper mantle: an analysis using quiet-day geomagnetic records of North America, *J. Geomag. Geoelectr.*, **35**, 367–382, 1983.

Campbell, W. H. and E. R. Schiffmacher, Upper mantle electrical conductivity for seven subcontinental regions of the Earth, *J. Geomag. Geoelectr.*, **40**, 1387–1406, 1988.

Campbell, W. H., E. R. Schiffmacher, and B. R. Arora, Quiet geomagnetic field representation for all days and latitudes, *J. Geomag. Geoelectr.*, **44**, 459–480, 1992.

Campbell, W. H., B. R. Arora, and E. R. Schiffmacher, External *Sq* currents in the India-Siberia region, *J. Geophys. Res.*, **98**, 3741–3752, 1993.

Chapman, S., The solar and lunar diurnal variation of the Earth's magnetism, *Phil. Trans. Roy. Soc. London*, **A218**, 1–118, 1919.

Chapman, S. and J. Bartels, *Geomagnetism*, Oxford University Press, Oxford, 1940.

Cleveland, W. S., Robust locally weighted regression and smoothing scatter plots, *J. Amer. Statistical Assn.*, **74**, 829–833, 1979.

Constable, S., Constraints on mantle electrical conductivity from field and laboratory measurements, *J. Geomag. Geoelectr.*, **45**, 1–22, 1993a.

Constable, S., Conduction by mantle hydrogen, *Nature*, **362**, 704, 1993b.

Duba, A., Are laboratory electrical conductivity data relevant to the Earth?, *Acta Geod. Geophys. Mont. Hung.*, **11**, 485–495, 1976.

Duba, A., What we really know of the electrical conductivity of mantle material?, *EOS Suppl.*, April 7, p. 298, 1992.

Duba, A. and von der Gönna, Comment on change of electrical conductivity of olivine associated with the olivine-spinal transition, *Phys. Earth Planet. Inter.*, **82**, 75–78, 1994.

Dziewonski, A. M. and D. L. Anderson, Preliminary reference Earth model, *Phys. Earth Planet. Inter.*, **25**, 297–356, 1981.

Fainberg, E. B. and N. M. Rotanova, Distribution of electrical conductivity and temperature in the interior of the Earth according to deep electromagnetic sounding, *Geomagn. Aeron.*, **14**, 603–607, 1974.

Gasparik, T., The role of volatiles in the transition zone, *EOS Suppl.*, **72**, 498–499, 1991.

Gauss, C. F., Allgemeine Theorie des Erdmagnetismus, in Resultate aus den Beobachtungen des magnetischen Vereins im Yahr 1838, edited by C. F. Gauss and W. Weber, translated from the German by E. Sabine and R. Taylor, *Sci. Mem. Select, Trans. Foreign Acad. Learned Soc. Foreign J.*, **2**, 184–251, 1841.

Hobbs, B. A., Conductivity profiles from global data, *PAGEOPH*, **125**, 393–407, 1887.

Hwang, H. G. and B. Mitchell, Shear velocities, QB and the frequency dependance of QB in stable and tectonically active regions from surface wave observations, *Geophys. J. R. astr. Soc.*, **90**, 575–613, 1987.

Jones, A. G., Observations of the electrical asthenosphere beneath Scandinavia, *Tectonophys.*, **90**, 37–55, 1982.

Jones, A. G., On the equivalence of the "Neblett" and "Bostick" transformations, *J. Geophysics*, **53**, 72–73, 1983.

Karato, S., The role of hydrogen in the electrical conductivity of the upper mantle, *Nature*, **347**, 272–273, 1990.

Katsura, T. and E. Ito, The system Mg_2SiO_4-Fe_2SiO_4 at high pressures and temperatures: precise determination of stabilities of olivine, modified spinel and spinel, *J. Geophys. Res.*, **94**, 15,663–15,670, 1989.

Kennett, B. L. N. and E. R. Engdahl, Traveltimes for global Earthquake location and phase identification, *Geophys. J. Int.*, **105**, 429–465, 1991.

Matsushita, S. and H. Maeda, On the geomagnetic quiet solar daily variation field during the IGY, *J. Geophys. Res.*, **70**, 2535–2558, 1965.

Maxwell, J. C., *Treatise on Electricity and Magnetism*, Cambridge University Press, Cambridge, 1873.

Mechie, J., A. V. Egorkin, K. Fuchs, T. Ryberg, L. Solodilov, and F. Wenzel, *P*-wave mantle velocity structure beneath norther Eurasia from long-range recordings along the profile Quartz, *Phys. Earth Planet. Inter.*, **79**, 269–286, 1993.

Omura, K., Change of electrical conductivity of olivine associated with the olivine-spinel transition, *Phys. Earth Planet. Inter.*, **65**, 292–307, 1991.

Parkinson, W. D., The reliability of conductivity derived from diurnal variation, *J. Geomag. Geoelectr.*, **26**, 281–284, 1974.

Ram, A. and R. F. Mereu, Lateral variations in upper-mantle structure around India as obtained from Guaribidanur seismic array data, *Geophys. J. R. astr. Soc.*, **49**, 87–114, 1977.

Ram, A. and O. P. Singh, On the seismic structure of Indian upper-mantle regions, *Proc. Ind. Acad. Sci. (Earth and Planetary Sci.)*, **91**, 1–13, 1982.

Roberts, R. G., Global electromagnetic induction, *Surv. Geophys.*, **8**, 339–374, 1986.

Schmucker, U., An introduction to induction anomalies, *J. Geomag. Geoelectr.*, **22**, 9–33, 1970.

Schmucker, U., Electrical properties of the Earth's interior, *Numerical Data and Functional Relationships in Science and Technology: Geophysics of the Solid Earth, Moon and Planets*, edited by K. Fuchs and H. Suffel, pp. 370–397, Landolf-Bornstein New Series Group V, 2b, 1984.

Schmucker, U., Substitute conductors for electromagnetic response estimates, *Pure Appl. Geophys.*, **125**, 341–367, 1987.

Schultz, A. and J. Larsen, On the electrical conductivity of the midmantle: II. Delineation of heterogeneity by application of external inverse solutions, *Geophys. J. Int.*, **101**, 565–580, 1990.

Schuster, A., The diurnal variation of terrestrial magnetism, *Phil. Trans. Roy. Soc. London*, **A180**, 467–518, 1889.

Schuster, A., The diurnal variation of terrestrial magnetism, *Phil. Trans. Roy. Soc. London*, **A208**, 163–204, 1908.

Shankland, T. J. and H. S. Waff, Partial melting and electrical conductivity anomalies in the upper mantle, *J. Geophys. Res.*, **82**, 5409–5417, 1977.

Shankland, T. J., R. J. O'Connell, and H. G. Waff, Geophysical constraints on Partial melt in the upper mantle, *Rev. Geophys. Space Phys.*, **19**, 394–406, 1981.

Tarits, P., Electromagnetic studies of global geodynamic processes. 11th workshop on electromagnetic induction in the Earth, Victoria University of Wellington, 26 August–2 September 1992, pp 7.1–7.21, 1992.

Weidelt, P. W., W. Losecke, and K. Knodel, DIE BOSTICK transformation, in *Protokoll uber der Kolloquium Electromagnetische Tiefenforschun*, edited by V. Haak and J. Homilius, pp. 227–230, Berlin-Hannover, 1980.